Applied Catalysis B: Environmental 111–112 (2012) 621–627

Contents lists available at SciVerse ScienceDirect

Applied Catalysis B: Environmental

journal homepage: www.elsevier.com/locate/apcatb

Zn-containing ionic liquids bearing dialkylphosphate ligands for the coupling reactions of epoxides and CO_2

Jin Kyu Lee[a,1], Young Jin Kim[a,1], Young-Seop Choi[a], Hyunjoo Lee[b], Je Seung Lee[a], Jongki Hong[c], Eun-Kyung Jeong[c], Hoon Sik Kim[a,*], Minserk Cheong[a,**]

[a] Department of Chemistry and Research Institute of Basic Sciences, Kyung Hee University, 1 Hoegi-dong, Dongdaemoon-gu, Seoul 130-701, Republic of Korea
[b] Environment and Process Division, Korea Institute of Science and Technology, Seoul 136-791, Republic of Korea
[c] College of Pharmacy, Kyung Hee University, 1 Hoegi-dong, Dongdaemoon-gu, Seoul 130-701, Republic of Korea

ARTICLE INFO

Article history:
Received 13 July 2011
Received in revised form 3 October 2011
Accepted 2 November 2011
Available online 15 November 2011

Keywords:
Carbon dioxide utilization
Cyclic carbonates
Ionic liquids
Zinc bromide
Epoxides

ABSTRACT

Zn-containing room temperature ionic liquids (Zn-RTILs), prepared from the reactions of $ZnBr_2$ with 1-alkyl-3-methylimidazolium dialkyphosphates ([RMIm][R_2PO_4]), were highly active for the coupling reactions of CO_2 with epoxides, producing corresponding cyclic carbonates in high yields. FAB-mass spectral and computational results suggest that $[ZnBr(R_2PO_4)_2]^-$ could be an active species for the coupling reaction. Decomposition of cyclic carbonates into epoxides and CO_2 during the product recovery process via vacuum distillation was almost negligible even in the presence of a Zn-RTIL up to 130 °C.

1. Introduction

The transformation of CO_2 into 5-membered cyclic carbonates through the coupling reaction with epoxides is one of the most effective ways to utilize CO_2, a green house gas [1,2]. Cyclic carbonates are valuable chemicals that are being widely used as electrolyte components of lithium ion batteries, monomers of polycarbonates, aprotic polar solvents, paint strippers, adhesives, cosmetics, and reactants for many chemical reactions [3–6]. Since the first commercialization of cyclic carbonates from the coupling reactions using KI in 1950s, tremendous effort has been devoted to search for active catalysts to meet the increasing demand of cyclic carbonates. As a result, a large number of catalysts and catalytic systems have been developed, including phosphonium iodide, transition metal complexes, supported metal complexes, electroreduction, and ionic liquids (ILs) [7–17]. It has also been reported that ILs bearing a zinc tetrahalide anion, prepared from the reaction of zinc halides and an ILs with a halide anion, exhibit surprisingly high activities toward the coupling reactions [18–20]. The improvement of the catalytic activity has been significant with the discovery of the afore-mentioned Zn-containing ILs. However, the practical application of these catalysts has been restricted because cyclic carbonates are found to decompose into epoxide and CO_2 in the presence of an IL bearing a zinc tetrahalide anion during the product recovery process via vacuum distillation at elevated temperature [21,22]. Catalyst decomposition is another problem encountered in the synthesis of cyclic carbonates, which inevitably produces unwanted side products [23]. To circumvent these problems, it is desirable to develop new types of active and stable catalysts that are highly active for the coupling reaction of epoxides and CO_2, but almost inert to the decomposition reactions of cyclic carbonates. The catalyst for the coupling reaction is also capable of catalyzing the decomposition of cyclic carbonates into epoxides and CO_2, especially at elevated temperatures in the absence of CO_2 pressure. For this reason, a considerable loss of cyclic carbonates is often observed during the recovery of a cyclic carbonate from a catalyst-containing reaction mixture through vacuum distillation process.

For the decomposition to take place, there should exist a substantial interaction between the cyclic carbonate and the catalyst. Therefore, to prevent the decomposition, the catalyst should be designed in a way to minimize the interaction with cyclic carbonate. As an approach to reach this goal, we have attempted to use imidazolium-based zinc containing ILs bearing dialkylphosphate ligands as catalysts for the coupling reactions of epoxide with CO_2.

* Corresponding author. Tel.: +82 961 0432; fax: +82 2 959 6443.
** Corresponding author. Tel.: +82 2 961 0239; fax: +82 2 966 3701.
E-mail addresses: khs2004@khu.ac.kr (H.S. Kim), mcheong@khu.ac.kr (M. Cheong).
[1] These authors equally contributed.

0926-3373/$ – see front matter © 2011 Elsevier B.V. All rights reserved.
doi:10.1016/j.apcatb.2011.11.015

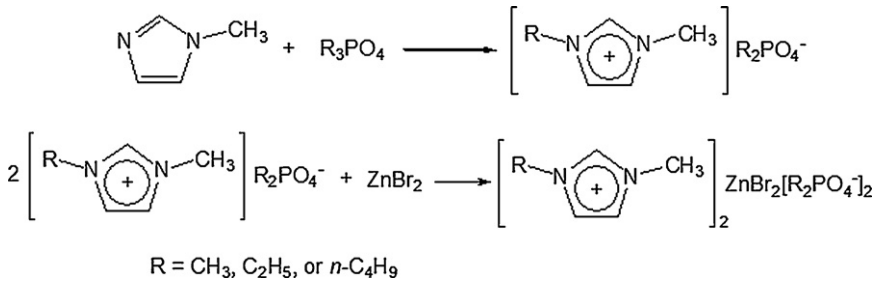

Scheme 1. Synthesis of Zn-RTILs.

It is hoped that the presence of bulky and chelating dialkylphosphate ligands on the zinc atom could play a role in limiting the interaction between the catalyst and cyclic carbonate as well as in enhancing the catalyst stability.

In this paper, we report the synthesis of Zn-containing room temperature ionic liquids (Zn-RTILs) from the reaction of $ZnBr_2$ with 1-alkyl-3-methylimidazolium dialkylphosphate ([RMIm][R_2PO_4]; R = C_1–C_4 alkyl) as illustrated in Scheme 1 and their catalytic activities for the coupling reactions of CO_2 with epoxides (see Scheme 2). The catalytic roles of Zn-RTILs for the coupling reactions and for the decomposition of ethylene carbonate (EC) have also been discussed in detail on the basis of experimental, spectroscopic, and computational calculations.

2. Experimental

2.1. General

Propylene oxide (PO) and all other chemicals to prepare Zn-RTILs were purchased from Aldrich Chemical Co. and were used without further purification, unless otherwise stated. Solvents were freshly distilled before use according to the literature procedures [24]. Ethylene oxide (EO) and CO_2 were obtained from Honam Petrochemical Co. and Sin Yang Gas Co., respectively, and used as received. [RMIm][R_2PO_4] were prepared according to the literature procedure by reacting 1-methylimidazole with corresponding trialkylphosphates [25,26].

^{1}H spectra were recorded on a Varian Unity 400 spectrometer. Fourier Transform Infrared (FT-IR) spectra were recorded on a Nicolet 380 spectrophotometer (Thermo Electron Co.). To avoid contact with water and air, FT-IR measurements were performed using a specially designed IR cell equipped with two KRS-5 windows (see the Supplementary data).

2.2. Synthesis of Zn-RTILs

Zn-RTILs were prepared by reacting anhydrous $ZnBr_2$ with [RMIm][R_2PO_4] at 100 °C. In a typical experiment, $ZnBr_2$ (2.25 g, 10 mmol) was reacted with [EMIm][Et_2PO_4] (5.29 g, 20 mmol) at 100 °C for 1 h to afford bis(1-ethyl-3-methylimidazolium) dibromobis(dimethylphosphato)zinc ([EMIm]$_2$[Br_2Zn(Et_2PO_4)$_2$]) as a transparent viscous liquid.

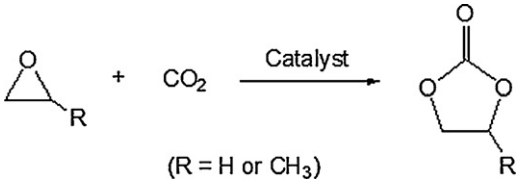

Scheme 2. Coupling reaction of CO_2 with epoxide.

Other Zn-RTILs were prepared in an analogous manner to that employed for the synthesis of [EMIm]$_2$[Br_2Zn(Et_2PO_4)$_2$].

2.3. FAB-mass spectral analysis of Zn-RTILs

FAB-mass spectra for the characterization of Zn-containing ILs were recorded with a JMS-700 Mstation double focusing mass spectrometer (JEOL, Tokyo, Japan) using a MS-MP9020D data system. The ion source was operated at 10 kV accelerating voltage with a mass resolution of 1500 (10% valley). Fast atoms were produced by FAB using a xenon atom gun operated at 6 keV. Samples were dissolved in methanol and mixed with 1 μL of 3-nitrobenzyl alcohol (NBA, Sigma, St. Louis, MO, USA) on a FAB probe tip.

2.4. Coupling reactions

All the coupling reactions were conducted in a 100 mL stainless-steel bomb reactor equipped with a magnet bar and an electrical heater. The reactor was loaded with an appropriate Zn-RTIL and an epoxide, and pressurized with CO_2 (1.5 MPa). The reactor was then heated to a specified reaction temperature and the pressure was maintained constant at 3.4 MPa by means of a CO_2 reservoir cylinder equipped with a high pressure regulator. After the completion of the reaction, volatiles were removed using an aspirator and the remaining product mixture was analyzed by a Hewlett Packard 6890 gas chromatograph equipped with a flame ionized detector and a DB-wax column (30 m × 0.32 mm × 0.25 μm), and a Hewlett Packard 6890-5973 MSD GC–mass spectrometer. For GC and GC–mass analysis, product mixture (1 g) was dissolved in methylene chloride (5 mL) and passed through a short silica gel or alumina column to remove small amounts of Zn-RTIL catalyst.

2.5. Quantum mechanical calculations

The formations of dibromodimethylphosphatozinc ([Br_2Zn(Me_2PO_4)]$^-$, [**Zn–P$_1$**]$^-$) and 1,3-dimethylimidazolium dibromobis(dimethylphosphato)zinc ([DMIm][Br_2Zn(Me_2PO_4)$_2$]$^-$, [**Zn–P$_2$**]$^-$) from $ZnBr_2$ and [DMIm][Me_2PO_4], and the coupling reaction of EO and CO_2 in the presence of [**Zn–P$_2$**]$^-$ were theoretically investigated using a Gaussian 03 program [27]. The geometry optimizations and thermodynamic corrections were performed with hybrid Becke 3-Lee–Yang–Parr (B3LYP) exchange-correlation functional with the 6–31 + G^* basis sets for C, H, N, O, and LanL2DZ(ECP) for Zn, P, and Br. In order to obtain the most stable geometries, all kinds of possible interaction patterns were optimized. No restrictions on symmetries were imposed on the initial structures. All stationary points were verified as minima by full calculation of the Hessian and a harmonic frequency analysis. For comparison, calculation on the formations of neutral Zn-RTILs, 1-3-dimethylimidazolium dibromodimethylphosphatozinc ([DMIm][Br_2Zn(Me_2PO_4)], **Zn–L**) and bis(1,3-dimethylimidazoloim) dibromobis(dimethylphosphato)zinc ([DMIm]$_2$[Br_2Zn(Me_2PO_4)$_2$], **Zn–2L**) were also conducted.

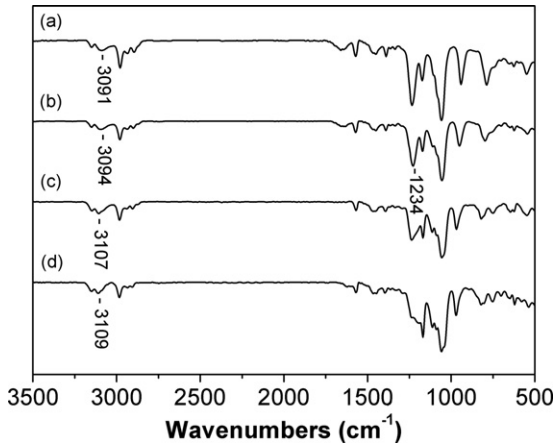

Fig. 1. FT-IR spectra of [EMIm][Et_2PO_4] and Zn-RTILs of various molar ratios of ZnBr/[EMIm][Et_2PO_4]: (a) [EMIm][Et_2PO_4], (b) 0.5, (c) 1, and (d) 1.5.

2.6. Decomposition tests

All of the decomposition tests were performed in a 100 mL 316 stainless steel reactor equipped with a magnet bar, an electric heater, a thermocouple, and a 316 stainless steel condenser. The condenser on the lid of the reactor was attached to a digital pressure gauge, which was connected directly to a vacuum pump. The bomb was charged with an appropriate catalyst and ethylene carbonate (EC) as the solvent and heated to a specified temperature. At the desired temperature, the reactor was evacuated to reduce the pressure to 1 mmHg by means of the vacuum pump. The degree of EC decomposition was monitored by the pressure increase during 5 min at the same temperature.

3. Results and discussion

3.1. Characterization of Zn-RTILs

3.1.1. FT-IR

Zn-RTILs were obtained as viscous liquids from the reactions of $ZnBr_2$ with [RMIm][R_2PO_4] at 100 °C for 1 h in the absence of a solvent. To confirm the formation of Zn-RTILs from $ZnBr_2$ and [RMIm][R_2PO_4], FT-IR experiment was conducted with the samples prepared from [EMIm][Et_2PO_4] and $ZnBr_2$. The molar ratio of $ZnBr_2$/[EMIm][Et_2PO_4] was varied in the range 0.5–1.50.

Fig. 1 displays the FT-IR spectra of [EMIm][Et_2PO_4] and Zn-RTILs. The broad peak centered at 3091 cm^{-1} in the spectrum of [EMIm][Et_2PO_4] was assigned to the stretching frequencies of C(2)–H mixed with the hydrogen bond interaction between imidazolium C(2)–H and [Et_2PO_4]$^-$ [28,29]. Upon reaction with $ZnBr_2$, the broad peak at 3091 cm^{-1} started to shift to higher frequencies and the degree of peak shift increased with the increasing content of $ZnBr_2$, indicating that the hydrogen bond interaction between C(2)–H and [Et_2PO_4]$^-$ is weakened by the incorporation of $ZnBr_2$. This is reasonable because [Et_2PO_4]$^-$ coordinated to Zn center would have much weaker basicity than that of [EMIm][Et_2PO_4]. As a result, the hydrogen bond interaction of the coordinated [Et_2PO_4]$^-$ ligand with C(2)–H becomes weakened, while increasing the bond strength of C(2)–H. A noticeable change was also observed for the peaks corresponding to P=O bond. When [EMIm][Et_2PO_4] was interacted with $ZnBr_2$, the peak assigned to P=O bond of [EMIm][Et_2PO_4] at 1234 cm^{-1} started to broaden and weaken with the increasing content of $ZnBr_2$, indicating that [Et_2PO_4]$^-$ is bonded to $ZnBr_2$ through the oxygen atom of P=O.

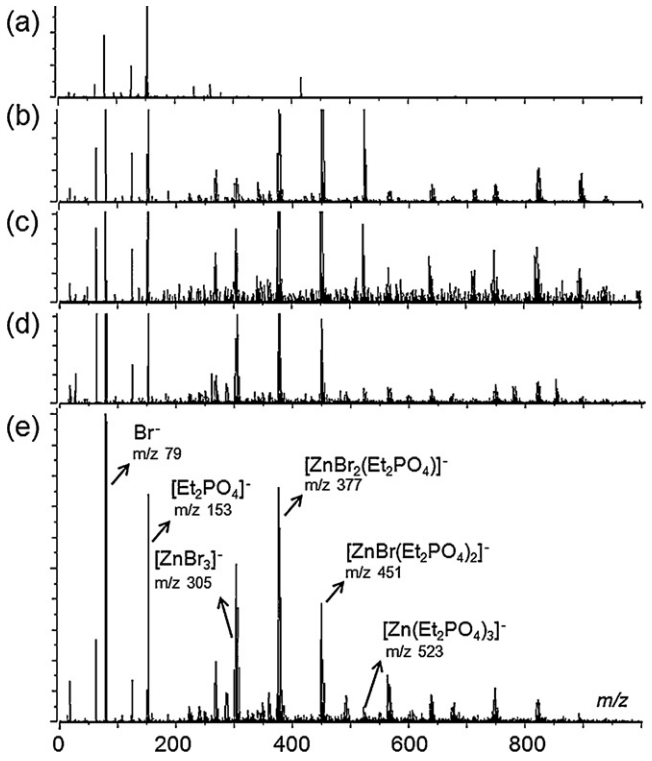

Fig. 2. FAB-mass spectra of [EMIm][Et_2PO_4] and Zn-RTILs of various molar ratios of $ZnBr_2$/[EMIm][Et_2PO_4]: (a) [EMIm][Et_2PO_4], (b) 0.3, (c) 0.5, (d) 1, and (e) 1.5.

3.1.2. ^1H NMR

The formation of Zn-RTILs was also investigated by ^1H and ^{31}P NMR spectroscopy. The chemical shift for C(2)–H of [EMIm][Et_2PO_4] at 9.828 ppm started to shift up-field with the incorporation of $ZnBr_2$, and the degree of shift increased with increasing content of $ZnBr_2$. This result indicates that the acidity for C(2)–H of [EMIm][Et_2PO_4] is reduced upon complexation with $ZnBr_2$. Contrary to C(2)–H, the chemical shift for CH_2 of ethyl group of [Et_2PO_4]$^-$ moved downfield by the complexation with $ZnBr_2$, demonstrating that there occurred a drastic change in the electronic environment of [Et_2PO_4]$^-$ (see Supplementary material, Fig. S-2).

3.1.3. FAB-mass spectral analysis of Zn-RTILs

To support the formation of Zn-RTILs, FAB-mass spectral analysis was undertaken with the four Zn-RTILs obtained from the reactions between $ZnBr_2$ and [EMIm][Et_2PO_4] in the molar ratios of $ZnBr_2$/[EMIm][Et_2PO_4] at 0.3, 0.5, 1, and 1.5. As shown in Fig. 2, various types of anionic zinc species are observed in the negative FAB-mass spectra of the Zn-RTILs, including [$ZnBr_3$]$^-$ (MW = 305), [$ZnBr_2(Et_2PO_4)$]$^-$ (MW = 377), [$ZnBr(Et_2PO_4)_2$]$^-$ (MW = 451), and [$Zn(Et_2PO_4)_3$]$^-$ (MW = 523). The relative peak intensity of each species varies significantly with the molar ratio of $ZnBr_2$/[EMIm][Et_2PO_4]. At the molar ratios of 1 and 1.5, the major anionic species are [$ZnBr_3$]$^-$, [$ZnBr_2(Et_2PO_4)$]$^-$, and [$ZnBr(Et_2PO_4)_2$]$^-$. By contrast, at the molar ratios of 0.3 and 0.5, the major anionic zinc species are found as [$ZnBr_2(Et_2PO_4)$]$^-$, [$ZnBr(Et_2PO_4)_2$]$^-$, and [$Zn(Et_2PO_4)_3$]$^-$. It is worth to note that the anionic species, [$ZnBr_2(Et_2PO_4)$]$^-$ and [$ZnBr(Et_2PO_4)_2$]$^-$ are commonly observed in the $ZnBr_2$/[EMIm][Et_2PO_4] molar ratio range of 0.3–1.5. Taken together, it is evident that Zn-RTILs are produced from the interaction of $ZnBr_2$ and [EMIm][Et_2PO_4], and Br of $ZnBr_2$ can be easily exchanged with [Et_2PO_4]$^-$.

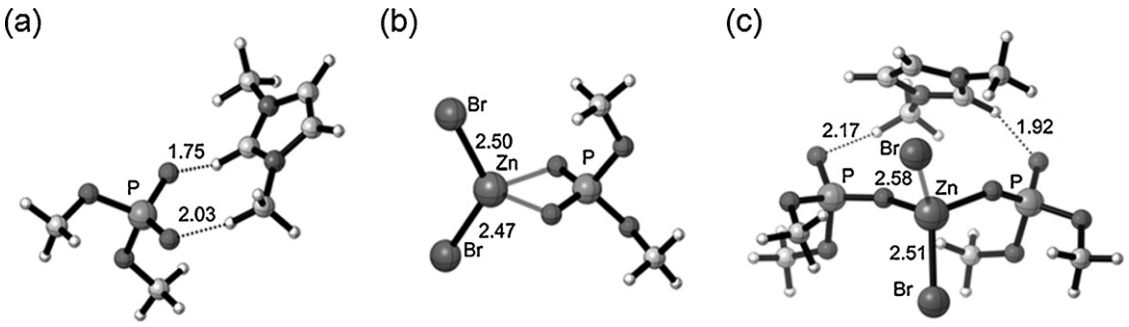

Fig. 3. Optimized structures showing the formation of $[\mathbf{Zn–P_2}]^-$ (c) from $[DMIm][Me_2PO_4]$ (a) and $[\mathbf{Zn–P_1}]^-$ (b). Gibbs free energy of formation of $[\mathbf{Zn–P_2}]^-$ is 15 kcal mol^{-1} lower than that of $[\mathbf{Zn–P_1}]^-$. $[\mathbf{Zn–P_1}]^-$: $[Br_2Zn(Me_2PO_4)]^-$, $[\mathbf{Zn–P_2}]^-$: $[DMIm][Br_2Zn(Me_2PO_4)_2]^-$.

3.2. Computational studies on the structures of Zn-RTILs

To have a deeper insight into the formation of Zn-RTILs, theoretical calculations on the interaction between $ZnBr_2$ and $[DMIm][Me_2PO_4]$ were carried out using Gaussian 03 program. All possible structures were considered to obtain the most stable geometries. Since we are only interested in the difference of stability between Zn ion with one $Me_2PO_4^-$ ligand and Zn ion with two $Me_2PO_4^-$ ligands to explain negative FAB-mass spectra of the Zn-RTILs, one $[DMIm]^+$ moiety was omitted in the calculation. Fig. 3 shows the optimized structures of the stable anionic zinc species, $[Br_2Zn(Me_2PO_4)]^-$ ($[\mathbf{Zn–P_1}]^-$) and $[DMIm][Br_2Zn(Me_2PO_4)_2]^-$ ($[\mathbf{Zn–P_2}]^-$) formed from the interactions of $ZnBr_2$ with one and two equivalents of $[DMIm][Me_2PO_4]$, respectively (see the Supplemendary data for the colored structures). Both $[\mathbf{Zn–P_1}]^-$ and $[\mathbf{Zn–P_2}]^-$ show stable tetrahedral arrangements of ligands around Zn, but there is a striking difference in the bonding mode of $[Me_2PO_4]^-$. In the optimized structure of $[\mathbf{Zn–P_1}]^-$, $[Me_2PO_4]^-$ ligand is coordinated to Zn in a chelating mode through two oxygen atoms. The calculated Gibbs free energy of formation (ΔG) of $[\mathbf{Zn–P_2}]^-$ was 15 kcal mol^{-1} lower than that of $[\mathbf{Zn–P_1}]^-$. This is a strong indication that the formation of $[\mathbf{Zn–P_2}]^-$ is much more favored than that of $[\mathbf{Zn–P_2}]^-$as long as sufficient amounts of $[DMIm][Me_2PO_4]$ is present. The Zn–Br bond distances of $[\mathbf{Zn–P_1}]^-$ and $[\mathbf{Zn–P_2}]^-$ are calculated as 250 and 260 pm, respectively. Considering the Zn–Br bond length of 221 pm for the vapor phase molecular $ZnBr_2$ [30], it is evident that Zn–Br bond distance of $ZnBr_2$ is significantly elongated on complexation with $[DMIm][Me_2PO_4]$. From the computational and FAB-mass spectral results, it is postulated that $[DMIm][Br_2Zn(Me_2PO_4)_2]^-$ is dissociated into [DMIm]Br and $[BrZn(Me_2PO_4)_2]^-$, a plausible active species.

To see the effect of cation–anion interaction on the stability of anionic zinc species, computational calculations were also conducted with the neutral compounds, **Zn–L** and **Zn–2L** by adding one $[DMIm][Me_2PO_4]$ to $[\mathbf{Zn–P_1}]^-$ and $[\mathbf{Zn–P_2}]^-$. The comparison of Gibbs free energies of formation of $[\mathbf{Zn–P_2}]^-$ and **Zn–2L** shows that ΔG of **Zn–2L** is only 1.5 kcal mol^{-1} lower than that of $[\mathbf{Zn–P_2}]^-$, implying that the stability of an anionic zinc species is not affected by the additional cation–anion interaction between [EMIm] and $Me_2PO_4^-$ ligand (see Supplementary material, Fig. S-3A and 3B).

3.3. Effect of catalyst composition

To find an optimal molar ratio of $ZnBr_2$/RTIL, the effect of catalyst composition on the catalytic activities of various Zn-RTILs was evaluated for the coupling reactions of CO_2 with PO or EO for 1 h with the molar ratios of EO/catalyst and PO/catalyst at 2000 and 1000, respectively. As shown in Table 1, both $[DMIm][Me_2PO_4]$ and $ZnBr_2$ exhibited negligible activities when they were used alone, but **Zn–2L**, prepared from the reaction of $ZnBr_2$ with two equivalents of $[DMIm][Me_2PO_4]$, showed a surprisingly high activity for the coupling reactions. Such a dramatic synergy effect can be most possibly attributed to the significant elongation of the Zn–Br bond from 221 to 260 pm when $ZnBr_2$ is complexed with two equivalents of $[DMIm][Me_2PO_4]$. As can be conceivable from the computational and FAB-mass spectral results, the lengthening of the Zn–Br bond seems to promote the dissociation of Br^- as [DMIm]Br from the Zn center of **Zn–2L**, thereby generating the vacant site for the coordination of an epoxide. In this context, the higher activity of **Zn–2L** than that of **Zn–L** can also be rationalized. As a whole, the catalytic activity of a Zn-RTIL, prepared from $ZnBr_2$ and $[DMIm][Me_2PO_4]$, increased sharply with decreasing molar ratio of $ZnBr_2$/$[EMIm][Et_2PO_4]$ down to 0.5 and remained almost constant on further decrease of the molar ratio. From this result, it is obvious that the molar ratio of $ZnBr_2$/$[EMIm][Et_2PO_4]$ should not exceed 0.5 for a Zn-RTIL to be used as an active catalyst for the coupling reactions.

It is widely accepted that the catalysts for the carboxylation of epoxides by CO_2 should possess both Lewis acidity and Lewis basicity [31]. It is also reported that the Lewis acidity of an Al-containing IL, prepared from $AlCl_3$ and [BMIm]Cl can be significantly altered by the variation of the molar ratio of $AlCl_3$/[BMIm]Cl: the higher the $AlCl_3$ content, the stronger the Lewis acidity [32]. In consideration of this, it is likely that the **Zn–2L** possesses the most suitable combination of Lewis acidity and basicity for the carboxylation.

3.4. Effect of alkyl substitution

As shown in Table 2, the catalytic activity of Zn-RTIL was somewhat affected by the degree of alkyl substitution on the imidazolium ring. Zn-RTIL with two or three alkyl groups on the imidazolium ring showed 10–20% higher activities than those containing one alkyl group on the imidazolium ring. These results

Table 1
Effect of catalyst composition on the coupling reactions of CO_2 and EO.[a]

Entry	Molar ratio	TOF (h^{-1})[b]	
	(ZnBr2/[DMIm][Me_2PO_4])	EO	PO
1	$[DMIm][Me_2PO_4]$	n.r.[c]	n.r.[c]
2	$ZnBr_2$	n.r.[c]	n.r.[c]
3	2.0	959	560
4	1.0 (**Zn–L**)	1345	702
5	0.67	1579	855
6	0.5 (**Zn–2L**)	1923	944
7	0.4	1937	949
8	0.3	1942	952

[a] Reactions were carried out at 100 °C and 3.5 MPa of CO_2 for 1 h. Molar ratios of epoxide/catalyst were set at 2000 for EO and 1000 for PO, respectively.
[b] TOF (h^{-1}): mole of cyclic carbonate/mole of catalyst/h.
[c] No reaction.

Table 2
Effect of alkyl substitution on the catalytic activities of Zn-RTILs for the coupling reactions of CO_2 and epoxides.[a]

Entry	Catalyst	TOF (h^{-1})[b]	
		EO	PO
1	$[DMIm]_2[Br_2Zn(Me_2PO_4)_2]$	1923	944
2	$[EMIm]_2[Br_2Zn(Et_2PO_4)_2]$	1928	945
3	$[BMIm]_2[Br_2Zn(Bu_2PO_4)_2]$	1935	953
4	$[EDMIm]_2[Br_2Zn(Et_2PO_4)_2]$	1984	991
5	$[BDMIm]_2[Br_2Zn(Bu_2PO_4)_2]$	1990	996
6	$[TMIm]_2[Br_2Zn(Me_2PO_4)_2]$	1977	988
7	$[MIm]_2[Br_2Zn(Me_2PO_4)_2]$	1626	832
8	$[EIm]_2[Br_2Zn(Et_2PO_4)_2]$	1779	863

[a] Reactions were carried out at 100 °C and 3.4 MPa of CO_2 for 1 h. Molar ratios of epoxide/catalyst were set at 2000 for EO and 1000 for PO, respectively.
[b] TOF (h^{-1}): mole of cyclic carbonate/mole of catalyst/h.

suggest that the electron donation from the alkyl group or groups to the imidazolium ring is of importance in the catalysis. On the contrary, the variation of alky group did not give any noticeable change in activity except for the Zn-RTIL with one alkyl group on the imidazolium ring. The reactivity was found in the order of increasing electron density on the imidazolium ring: 1-butyl-2,3-dimethylimidazolium dibutylphosphate ($[BDMIm][Bu_2PO_4]$) ~ 1-ethyl-2,3-dimethylimidazolium diethylphosphate ($[EDMIm][Et_2PO_4]$) ~ 1,2,3-trimethylimidazolium dimethylphosphate ($[TMIm][Me_2PO_4]$) > 1-butyl-3-methylimidazolium dibutylphosphate ($[BMIm][Bu_2PO_4]$) ~ 1-ethyl-3-methylimidazolium diethylphosphate ($[EMIm][Et_2PO_4]$) ~ 1,3-dimethylimidazolium dimethylphosphate ($[DMIm][Me_2PO_4]$) > 1-ethylimidazolium diethylphosphate ($[EIm][Et_2PO_4]$) > 1-methylimidazolium dimethylphosphate ($[MIm][Me_2PO_4]$).

3.5. Effects of temperature and pressure

The effects of temperature and pressure were also investigated in the presence of **Zn–2L**. The molar ratios of EO/catalyst and PO/catalyst were set at 5000 and 2000, respectively. As can be seen in Table 3, the TOF increased steeply with increasing temperature, but the effect of pressure was not pronounced. The TOF also increased with increasing molar ratio of epoxide/Zn-RTIL, but the % yield (100 × TOF/molar ratio) of cyclic carbonate decreased with the increase of the molar ratio (Table 4).

3.6. Computational studies on the mechanism

The mechanisms for the IL-catalyzed carboxylation of epoxides have been proposed by several groups [9,33–35], but detailed theoretical investigation has never been attempted. To elucidate the role

Table 3
Effects of temperature and pressure of CO_2 for the coupling reactions of CO_2 and epoxides catalyzed by $[DMIm]_2[Br_2Zn(Me_2PO_4)_2]$.[a]

Entry	T (°C)	P (MPa)	TOF (h^{-1})[b]	
			EO	PO
1	140	3.5	4989	1997
2	120	3.5	4212	1811
3	100	3.5	3356	1335
4	80	3.5	796	255
5	100	5.0	3441	1379
6	100	4.0	3423	1365
7	100	3.0	3006	1328
8	100	2.5	2977	1305
9	100	2.0	2970	1295

[a] Reactions were carried out at various temperatures and pressures of CO_2 for 1 h. Molar ratios of epoxide/catalyst were set at 5000 for EO and 2000 for PO, respectively.
[b] TOF(h^{-1}): mole of cyclic carbonate/mole of catalyst/h.

Table 4
Effects of molar ratio of epoxide/Zn-RTIL on the coupling reactions of epoxides and CO_2.[a]

Entry	Molar ratio (EO/Zn-RTIL)	Molar ratio (PO/Zn-RTIL)	TOF (h^{-1})[b]	
			EO	PO
1	6000	–	4788	–
2	4000	–	3455	–
3	3000	–	2851	–
4	2000	–	1998	–
5	1000	–	999	–
6	–	3000	–	2362
7	–	1500	–	1455
8	–	750	–	745
9	–	500	–	499

[a] Reactions were carried out at 120 °C and 3.5 MPa of CO_2 for 1 h in the presence of $[EMIm]_2[Br_2Zn(Et_2PO_4)_2]$, and the amounts of EO and PO were fixed at 0.5 moles, respectively.
[b] TOF (h^{-1}): mole of cyclic carbonate/mole of catalyst/h.

of Zn-RTIL more clearly and to have a clue on the design of better performance catalysts, we have conducted computational investigation on the carboxylation of EO in the presence of $[\mathbf{Zn–P_2}]^-$.

Fig. 4 shows the optimized structures for the interactions of EO with CO_2 in the presence of $[\mathbf{Zn–P_2}]^-$ (see the Supplementary materials, Fig. S-4A and 4B for the colored structures). The calculation shows that the production of ethylene carbonate proceeds in three steps. The first step is the coordination of EO to the Zn center of $[\mathbf{Zn–P_2}]^-$ along with the concomitant dissociation of Br^- as [DMIm]Br to generate **1** ($[BrZn(Me_2PO_4)_2(EO)]^-$ + [DMIm]Br). The driving force for the dissociation of Br^- is the strong interaction between C(2)–H of an imidazolium ring and a bromide ligand. The Gibbs free energy of formation ($\Delta G_{\mathbf{1}}$) of **1** was calculated as 5.1 kcal mol^{-1}.

The second step is the attack of the dissociated Br^- on the carbon atom of coordinated epoxide followed by the simultaneous ring opening, leading to the formation of an intermediate species **2**, $([DMIm][BrZn(Me_2PO_4)_2(OCH_2CH_2Br)])^-$. The activation energy ($\Delta G^{\ddagger}_{TS1}$) and the Gibbs free energy of formation of **2** ($\Delta G_{\mathbf{2}}$) were calculated as 18.5 and 10.4 kcal mol^{-1}, respectively. The third step involves CO_2 insertion into the Zn–O bond of $Zn–OCH_2CH_2Br$ to generate **3**, $([DMIm][BrZn(Me_2PO_4)_2(OCO_2CH_2CH_2Br)])^-$ ($\Delta G_{\mathbf{3}}$ = 7.5 kcal mol^{-1}). Although there is no transition state (TS) for the CO_2 insertion step, formation of an intermediate CO_2 adduct is observed, in which CO_2 interacts with the oxygen atom of ethoxy ligand (see Supplementary Material, Fig. S-4C). The Gibbs free energy of formation of the CO_2 adduct is 5.7 mol^{-1} higher than that of the species **2**. The CO_2 insertion into the Zn–O bond seems to occur spontaneously as soon as CO_2 adduct is formed. The final step is the interaction of carbonate oxygen atom with the carbon atom of CH_2Br along with the simultaneous C–Br bond lengthening (TS2, $\Delta G^{\ddagger}_{TS2}$ = 19.9 kcal mol^{-1}) and the ring closing to form ethylene carbonate-coordinated species **4**, ($[BrZn(Me_2PO_4)_2(EC)]^-$ + [DMIm]Br) ($\Delta G_{\mathbf{4}}$ = –2.1 kcal mol^{-1}). For clarity, energy diagram for the catalytic cycle is shown in Fig. 5. Taken together, it is likely that the rate-determining step is the ring closing step because $\Delta G^{\ddagger}_{TS2}$ is slightly higher than $\Delta G^{\ddagger}_{TS1}$ for the ring opening step. Nonetheless, it seems more reasonable to assume that both steps are equally affecting the rate of carboxylation because the difference in activation energy is only 1.4 kcal mol^{-1}.

3.7. EC decomposition test

Decomposition tests were conducted under a reduced pressure of 1 mmHg to compare the EC decomposition rate in the presence of **Zn–2L** with that in the presence of $[DMIm]_2[ZnCl_2Br_2]$, one of the most active catalysts so far reported for the coupling reactions

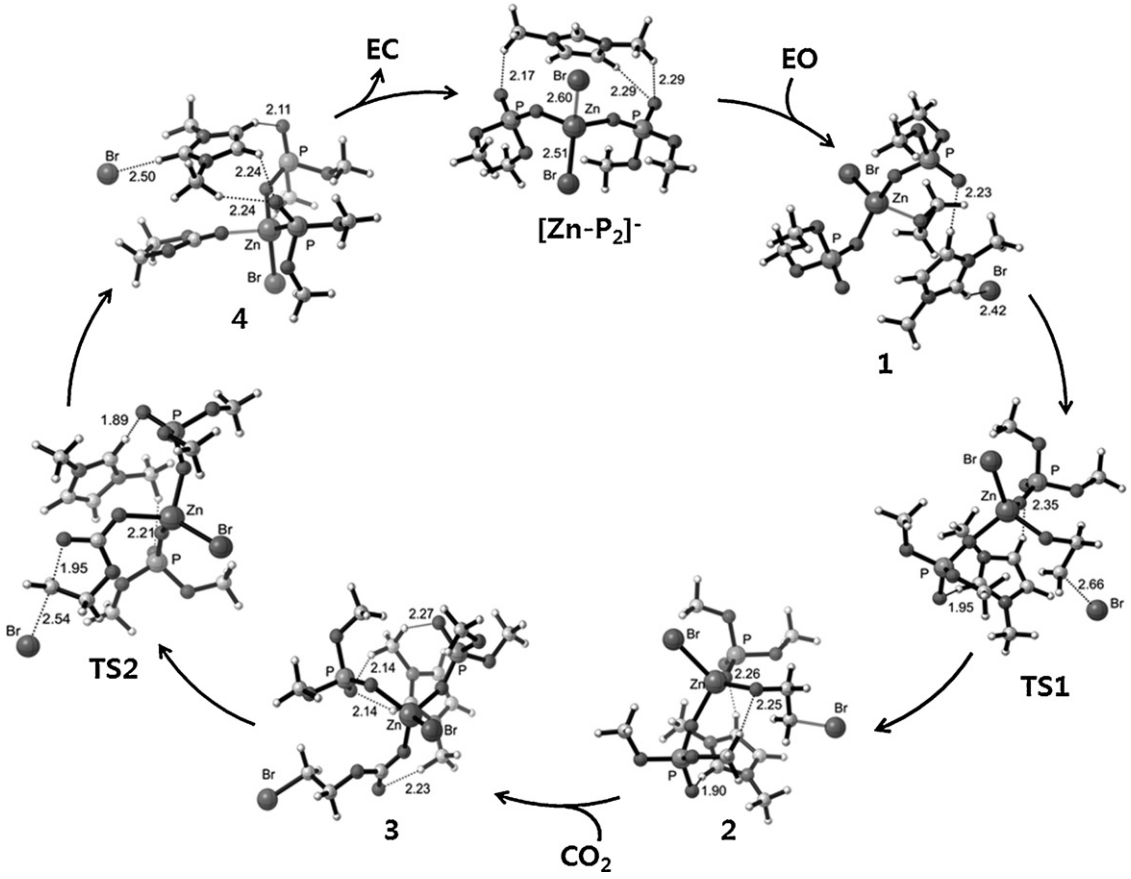

Fig. 4. Optimized structures of reaction intermediates and transition states involved in the coupling reaction of EO with CO_2 in the presence of an active species, [**Zn–P$_2$**]$^-$: $\Delta G^{\ddagger}_{\mathbf{TS1}} = 18.5$ kcal mol^{-1}, $\Delta G^{\ddagger}_{\mathbf{TS2}} = 19.9$ kcal mol^{-1}, $\Delta G_{\mathbf{1}} = 5.1$ kcal mol^{-1}, $\Delta G_{\mathbf{2}} = 10.4$ kcal mol^{-1}, $\Delta G_{\mathbf{3}} = 7.5$ kcal mol^{-1}, $\Delta G_{\mathbf{4}} = -2.1$ kcal mol^{-1}. The Gibbs free energy of formation (ΔG) and transition state energy ($\Delta G^{\ddagger}$) are relative values with respect to that of the reactant. **1**: [$BrZn(Me_2PO_4)_2(EO)]^-$ + [DMIm]Br, **2**: ([DMIm][$BrZn(Me_2PO_4)_2(OCH_2CH_2Br)$])$^-$, **3**: ([DMIm][$BrZn(Me_2PO_4)_2(OCO_2CH_2CH_2Br)$])$^-$, **4**: [$BrZn(Me_2PO_4)_2(EC)]^-$ + [DMIm]Br.

of epoxide and CO_2. The catalyst concentration was set at 0.1 wt.% with respect to EC. As displayed in Fig. 6, no EC decomposition was observed up to 150 °C in the absence of a catalyst. However, in the presence of 0.1 wt.% $[DMIm]_2[ZnCl_2Br_2]$, EC started to decompose at 95 °C. The rate of decomposition was slow up to 130 °C, but increased steeply on further increase of temperature. On the contrary, the rate of EC decomposition was much slower in the presence of **Zn–2L**. The reason for the slowdown of the EC decomposition with **Zn–2L** is not clear at the moment, but it is postulated that the bulky $[Me_2PO_4]^-$ ligands might play a role in preventing the interaction of **Zn–2L** with EC. If this is the case, the activity of Zn-based catalysts toward the decomposition of alkylene carbonates could be suppressed to a great extent through a suitable ligand design.

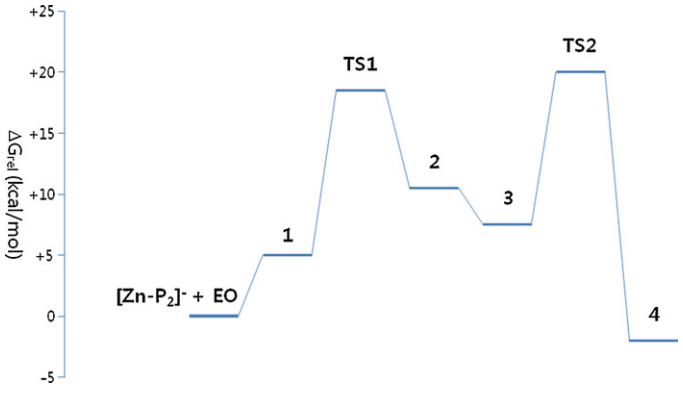

Fig. 5. Calculated free energy profile for the coupling reaction of EO with CO_2 in the presence of [**Zn–P$_2$**]$^-$. [**Zn–P$_2$**]$^-$: [DMIm][$Br_2Zn(Me_2PO_4)_2]^-$, **1**: [$BrZn(Me_2PO_4)_2$(EO)]$^-$ + [DMIm]Br, **2**: ([DMIm][$BrZn(Me_2PO_4)_2(OCH_2CH_2Br)$])$^-$, **3**: ([DMIm][$BrZn(Me_2PO_4)_2(OCO_2CH_2CH_2Br)$])$^-$, **4**: [$BrZn(Me_2PO_4)_2(EC)]^-$ + [DMIm]Br.

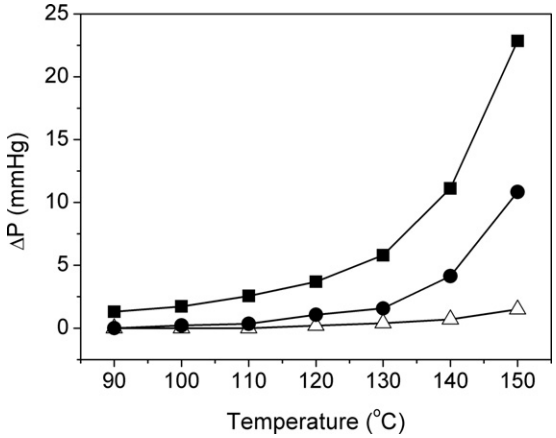

Fig. 6. Effect of temperature on the EC decomposition with or without the presence of a Zn-RTIL catalyst: (△) pure EC, (■) 0.1 wt.% $[DMIm]_2ZnBr_2Cl_2$, (●) 0.1 wt.% **Zn–2L** ($[DMIm]_2[ZnBr_2(Me_2PO_4)_2]$).

4. Conclusions

We have demonstrated that the Zn-RTILs prepared from $ZnBr_2$ and dialkylimidazolium dialkylphosphate are highly active catalyst for the cycloaddition of CO_2 with EO and PO, producing EC and PC in high yields. More advantageously, the decomposition of EC during the product recovery process via vacuum distillation was greatly reduced in the presence of **Zn–2L**. Computational study on the mechanism for the coupling reaction in the presence of $[\mathbf{Zn–P_2}]^-$ shows that $[Me_2PO_4]^-$ ligands coordinated to Zn center play a pivotal role in assisting the dissociation of Br^- from the Zn center. We believe that the mechanistic details present in this study may provide valuable information to those wish to develop high performance catalysts for the coupling reactions of epoxides and CO_2.

Acknowledgements

We acknowledge the financial support by grants (AC3-101) from Carbon Dioxide Reduction & Sequestration Research Center, one of the 21st Century Frontier Programs funded by the Ministry of Science and Technology of Korean government.

Appendix A. Supplementary data

Supplementary data associated with this article can be found, in the online version, at doi:10.1016/j.apcatb.2011.11.015.

References

[1] T. Sakakura, J.C. Choi, H. Yasuda, Chem. Rev. 107 (2007) 2365–2387.
[2] J.L. Wang, C.X. Miao, X.Y. Dou, J.A. Gao, L.N. He, Curr. Org. Chem. 15 (2011) 621–646.
[3] A.A. Shaikh, S. Sivaram, Chem. Rev. 96 (1996) 951–976.
[4] M. Inaba, Z. Siroma, A. Funabiki, Z. Ogumi, Langmuir 12 (1996) 1535–1540.
[5] J.H. Clements, Ind. Eng. Chem. Res. 42 (2003) 663–674.
[6] L. Han, H.J. Choi, S.J. Choi, B.Y. Liu, D.W. Park, Green Chem. 13 (2011) 1023–1028.
[7] J.J. Peng, Y.Q. Deng, New J. Chem. 25 (2001) 639–641.
[8] H. Kawanami, A. Sasaki, K. Matsui, Y. Ikushima, Chem. Commun. (2003) 896–897.
[9] H.S. Kim, J.Y. Bae, J.S. Lee, O.-S. Kwon, P. Jelliarko, S.D. Lee, S.-H. Lee, J. Catal. 232 (2005) 80–84.
[10] J. Sun, L. Wang, S.J. Zhang, Z.X. Li, X.P. Zhang, W.B. Dai, R.H. Mori, J. Mol. Catal. A: Chem. 256 (2006) 295–300.
[11] S.J. Zhang, Y.H. Chen, F.W. Li, X.M. Lu, W.B. Dai, R. Mori, Catal. Today 115 (2006) 61–69.
[12] F. Ono, K. Qiao, D. Tomida, C. Yokoyama, J. Mol. Catal. A: Chem. 263 (2007) 223–226.
[13] A. Zhu, T. Jiang, B. Han, J. Zhang, Y. Xie, X. Ma, Green Chem. 9 (2007) 169–172.
[14] S.L. Zhang, Y.Z. Huang, H.W. Jing, W.X. Yao, P. Yan, Green Chem. 11 (2009) 935–938.
[15] K.M.K. Yu, I. Curcic, J. Gabriel, H. Morganstewart, S.C. Tsang, J. Phys. Chem. A 114 (2010) 3863–3872.
[16] B. Eneau-Innocent, D. Pasquier, F. Ropital, J.M. Leger, K.B. Kokoh, Appl. Catal. B: Environ. 98 (2010) 65–71.
[17] S.G. Liang, H.Z. Liu, T. Jiang, J.L. Song, G.Y. Yang, B.X. Han, Chem. Commun. 47 (2011) 2131–2133.
[18] H.S. Kim, J.J. Kim, H. Kim, H.G. Jang, J. Catal. 220 (2003) 44–46.
[19] J. Palgunadi, O.S. Kwon, H. Lee, J.Y. Bae, B.S. Ahn, N.Y. Min, H.S. Kim, Catal. Today 98 (2004) 511–514.
[20] J.M. Sun, S.I. Fujita, F.Y. Zhao, M. Arai, Appl. Catal. A: Gen. 287 (2005) 221–226.
[21] S. Fujita, B.M. Bhanage, Y. Ikushima, M. Shirai, K. Torii, M. Arai, Catal. Lett. 79 (2002) 95–98.
[22] H.S. Kim, P. Jelliarko, J.S. Lee, S.Y. Lee, H. Kim, S.D. Lee, B.S. Ahn, Appl. Catal. A: Gen. 288 (2005) 48–52.
[23] H. Okamoto, Method of manufacturing alkylene carbonate, EP 1630161, 2006.
[24] W.L.F. Armarego, C.L.L. Chai, Purification of Laboratory Chemicals, 5th ed., Elsevier, 2003.
[25] C.J. Bradaric, A. Downard, C. Kennedy, A.J. Robertson, Y.H. Zhou, Green Chem. 5 (2003) 143–152.
[26] E. Kuhlmann, S. Himmler, H. Giebelhaus, P. Wasserscheid, Green Chem. 9 (2007) 233–242.
[27] M.J. Frisch, G.W. Trucks, H.B. Schlegel, et al., Gaussian 03, Revision C.02, Gaussian Inc., Pittsburgh, PA, 2004.
[28] Y. Shiraishi, K. Tachibana, T. Hirai, I. Komasawa, Ind. Eng. Chem. Res. 40 (2001) 4919–4924.
[29] Y.J. Kim, R.S. Varma, J. Org. Chem. 70 (2005) 7882–7891.
[30] A.F. Wells, Structural Inorganic Chemistry, 5th ed., Oxford Science Publications, 1984.
[31] H. Kisch, R. Millini, I.-J. Wang, Chem. Ber. 119 (1986) 1090–1093.
[32] C.L. Hussey, Pure Appl. Chem. 60 (1988) 1763–1772.
[33] X.B. Lu, R. He, C.X. Bai, J. Mol. Catal. A: Chem. 186 (2002) 1–11.
[34] L.F. Xiao, F.W. Li, J.J. Peng, C.G. Xia, J. Mol. Catal. A: Chem. 253 (2006) 265–269.
[35] W.L. Dai, L. Chen, S.F. Yin, S.L. Luo, C.T. Au, Catal. Lett. 135 (2010) 295–304.